Nano Energy 40 (2017) 587–595

Contents lists available at ScienceDirect

Nano Energy

journal homepage: www.elsevier.com/locate/nanoen

Full paper

$NaNbO_3$ two-dimensional platelets induced highly energy storage density in trilayered architecture composites

Zhongbin Pan[a], Baihui Liu[a], Jiwei Zhai[a,*], Lingmin Yao[b], Ke Yang[a], Bo Shen[a]

[a] Key Laboratory of Advanced Civil Engineering Materials, Ministry of Education, School of Materials Science & Engineering, Tongji University, 4800 Caoan Road, Shanghai 201804, China

[b] School of Physics and Electronic Engineering, Guangzhou University, Guangzhou 510006, China

ARTICLE INFO

Keywords:
Energy density
Dielectric properties
Capacitors
Composite films
Finite element simulation

ABSTRACT

Polymer-based dielectric materials with high power density, high energy density, and broad operating temperature range are critical to the development of cost-efficient and lightweight capacitors for modern high-power electrical systems. Here, $NaNbO_3$ (NN)/polymer composites, especially two-dimensional (2D) NN platelets, were used to create new composite films for energy storage applications for the first time. The trilayered architecture composites comprised of two outer layers of 2D NN platelets dispersed in a poly(vinylidene fluoride) (PVDF) matrix to provide high dielectric constant and a middle layer of pristine PVDF to offer high breakdown strength. The breakdown strength and energy density of the trilayered architecture composite films were improved significantly via tailoring the contents of the 2D NN platelets. The composite films with an optimized filler content illustrate a high discharge energy density of 13.5 J cm^{-3} at 400 MV m^{-1}, far more than the best commercial biaxially- oriented polypropylenes. Moreover, the composite films show a superior power density of 2.68 MW cm^{-3} and ultra-fast discharge speed of 0.127 μs. Finite element simulation further revealed the breakdown strength and energy density of the composite films were much enhanced compared to the corresponding single layer composite films. Therefore, the new trilayered architecture composite films can be applied as an alternative promising high-performance electrostatic capacitor material.

1. Introduction

The ever-growing market of dielectric materials demands higher performance and more efficient dielectrics with improved functionality and low cost [1–4]. Lightweight, compact and high-energy-density capacitors are highly demanded by mobile electronic devices, hybrid electric vehicles, medical implants and other technologies [5–10]. One of the important merits used to quantify capacitor performance is the energy stored density of a capacitor (U_e), computed as $U_e = \int E\mathrm{d}D$ [11–13], where E is the applied electric field and D is the electric displacement. To maximize the energy density, we have to optimize the dielectric breakdown strength and dielectric polarization. Usually, the energy density of a pristine polymer is limited by low dielectric permittivity (< 5) [14]. For instance, biaxially-oriented polypropylene (BOPP), the best commercial high-pulse-discharge polymer capacitor, possesses relatively low energy density (< 4 J cm^{-3}) due to its low dielectric constant (≈ 2), which seriously limits its applications [15]. Therefore, polymer nanocomposites have gained significant attention with hypothesis that inorganic fillers in a polymer matrix could improve the overall dielectric performances by combining high-dielectric-constant inorganic nanomaterials and high-breakdown-strength polymer matrix [7,12,14,16–18].

The microstructural morphology and concentration of the filler play dominant roles in the energy storage density of polymer nanocomposites [19–27]. Compared with zero-dimensional (0D) fillers, one/two-dimensional (1/2D) high-aspect-ratio fillers at low concentration are more effective in enhancing the dielectric performances and energy density of polymer nanocomposites [28–34]. In addition, the small special surfaces of the large-aspect-ratio fillers possess further contribute to reducing surface energy and alleviating nanofiller agglomeration in the polymer matrix. Recently, we suggest that 1D $BaTiO_3$ nanofillers, after being introduced into the poly(vinylidene fluoride) (PVDF) matrix, outperform 0D $BaTiO_3$ nanoparticles in improving dielectric properties and energy density [29]. Compared with the 0D $BaTiO_3$ nanoparticles, nanocomposites loaded with 4 vol% 1D $BaTiO_3$ nanofibers exhibit larger dielectric constant (14.69 vs. 11.03 at 1 kHz), breakdown strength (300 vs. 370 MV m^{-1}), and energy density (8.78 vs. 4.86 J cm^{-3}) under the same conditions. As reported, the dielectric constant of nanocomposite films combined from $BaTiO_3$ nanowires and the PVDF matrix increased with the rising aspect ratio of the nanowires

* Corresponding author.
E-mail address: apzhai@tongji.edu.cn (J. Zhai).

http://dx.doi.org/10.1016/j.nanoen.2017.09.004
Received 13 June 2017; Received in revised form 30 August 2017; Accepted 2 September 2017
Available online 05 September 2017

[35]. Nanocomposites with 30 vol% $BaTiO_3$ nanowires and an aspect ratio of 45.8 can reach a dielectric constant of 44.3, which is 30.7% higher than samples with an aspect ratio of 9.3% and 352% larger than the polymer matrix [35]. Similarly, incorporation of 2D fillers in the polymer matrix could essentially increase breakdown strength and energy density [3,28–31,36]. The 2D fillers in the polymer matrix act as nucleating agents that promote the growth of nonpolar crystals in the vicinity since the mobility of the dipoles is restricted in these crystals. The high-aspect-ratio 2D fillers also build up efficient conduction barriers that limit the charge migration toward the electrodes and hider the growing electric tree during breakdown [28–31]. For instance, the breakdown strength, energy density, and discharge-charge efficiency of the poly(vinylidene fluoride-trifluoroethylene-chlorofluoroethylene terpolymer) matrix were remarkably improved upon the incorporation of ultra-thin 2D boron nitride nanosheets (BNNSs) [30]. This improvement could be ascribed to the build-up of efficient conduction barriers that limit the charge migration toward the electrodes and hider the growing electric tree during breakdown.

In particular, the dielectric constant and breakdown strength can be simultaneously improved by designing multilayered architecture composite films [37–44]. The dielectric properties and energy density of sandwich-structured ceramic/polymer nanocomposite films can be significantly improved by adjusting the filler content of the outer and middle layers. For instance, sandwich-structured nanocomposites shown much improved energy density, which resulted from the simultaneous improvement of dielectric constant (from 10 to 13 at 1 kHz) and breakdown strength (from 340 to 410 MV m^{-1}) [39]. Trilayered polymer nanocomposites with optimized content of the filler (2D BNNS nanosheets as outer layers and $Ba_{0.5}Sr_{0.5}TiO_3$ nanowires as middle layer) display a discharged energy density of 20.5 J cm^{-3} at Weibull breakdown strength of 588 MV m^{-1}, which is among the highest discharged energy densities reported so far [43]. The largest energy density is ascribed to specially designed geometric structure between the sandwich structure and high intrinsic breakdown strength (800 MV m^{-1}) [45]. But applications of the high-quality 2D ultra-thin BNNSs are largely limited by the low dielectric constant (~3–4) and complex preparation method [30,45].

The $NaNbO_3$ (NN) ceramic is an excellent lead-free ferroelectric ceramic with relatively high dielectric constant of ~ 300 at 1 kHz, and has attracted considerable attention as a potential replacement of lead-based piezoelectric materials [46–48]. However, research on using NN/polymer composites, especially 2D NN platelets, to create new nanocomposites for energy storage applications, has been reported rarely. In this study, high-aspect-ratio 2D NN platelets were prepared and used as fillers incorporated into the polymer matrix. Additionally, trilayered architecture composite films were designed, with the high-dielectric-constant NN/PVDF as two outer layers and the high-breakdown-strength pristine PVDF as the middle layer (Fig. 1). Experiments suggest the dielectric performances, energy density, and discharge efficiency of the composite films could be adjusted simultaneously by changing the 2D NN platelets contents in the outer layers. The trilayered architecture composite films with optimized filler content have a discharge energy density up to 13.5 J cm^{-3} at 400 MV m^{-1}, which is far larger than both commercial BOPP and pristine PVDF. The composite films show a superior power density of 2.68 MW cm^{-3} and ultra-fast discharge speed of 0.127 μs.

2. Experimental

2.1. Prepared $NaNbO_3$ (NN) two-dimensional platelets

$NaNbO_3$ (NN) two-dimensional platelets were synthesized by two-step melon salt process [37,39]. First, Bi_2O_3 (99.975%, Alfa Aesar) and Nb_2O_5 (99.9%, Alfa Aesar) were heated in a NaCl flux at 1000 °C for 2 h to form two-dimensional platelets $Bi_{2.5}Na_{3.5}Nb_5O_{18}$ (BiNN5) precursors. Next, the mixed BiNN5 and NaCl were reacted at 1000 °C for 2 h. The mixtures were washed by hot deionized water and HNO_3 several times, dried at 70 °C for 24 h. The as-synthesized NN two-dimensional platelets were then crushed in liquid nitrogen. The morphologies were characterized by high-resolution transmission electron microscope (HRTEM, Philips, Netherland) and field-emission scanning electron microscope (FESEM, XL30FEG).

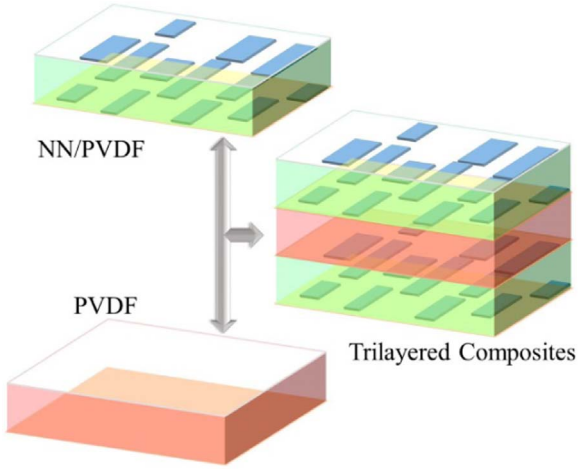

Fig. 1. Fabrication of trilayered architecture composite films.

2.2. Surface functionalization NN two-dimensional platelets

NN two-dimensional platelets were dispersed in 0.02 mol L^{-1} dopamine hydrochloride solutions (Shanghai Aladdin Industrial Inc.) under stirring at 60 °C for 12 h and then vacuum-dried at 80 °C for 10 h. The dense and robust surface layers of dopamine were observed by HRTEM and further evidenced by X-ray photoelectron spectroscopy (XPS).

2.3. Fabrication of nanocomposite films

First, the dopamine-coated NN two-dimensional platelets and PVDF (2 g) (Arkema, Kynars 301F) were proportionally dispersed into dimethylformamide (100 ml) for 2 h of ultrasonication and then stirred for at 70 °C for 24 h, forming a stable suspension. The NN/PVDF composite films were prepared via solution casting method on the ITO substrate, which were vacuum-dried at 60 °C for 10 h to volatilize the solvent. The trilayered architecture NN/PVDF composite films were prepared by solution casting layer by layer, which were vacuum-dried at 60 °C for 10 h to volatilize the solvent. The thickness of the trilayered architecture composite films could be controlled by the height of the casting scraper. All the samples were heated-treatment at 200 °C for 10 min and immediately quenched in ice-water to obtain dense composite films. After were vacuum-dried at 70 °C for 10 h to complete volatilize the residual water. The composite films morphologies were observed by FESEM.

2.4. Measurement of dielectric properties

Both of side composite films were sputtered with 60-nm-thick and 2-mm-diameter copper electrodes for electrical measurements. Their dielectric performance were characterized by an E4980A LCR meter (Agilent, Palo Alto, CA, USA) from frequency 10^3–10^6 Hz at 1000 mV and ambient temperature. The leakage current density was measured by Keithley 2400 source meter (Keithley Instruments, Inc.) at 100 MV m^{-1}. The D-E loops were characterized by a Premier II ferroelectric test system (Radiant Technologies Inc.) at 10 Hz.

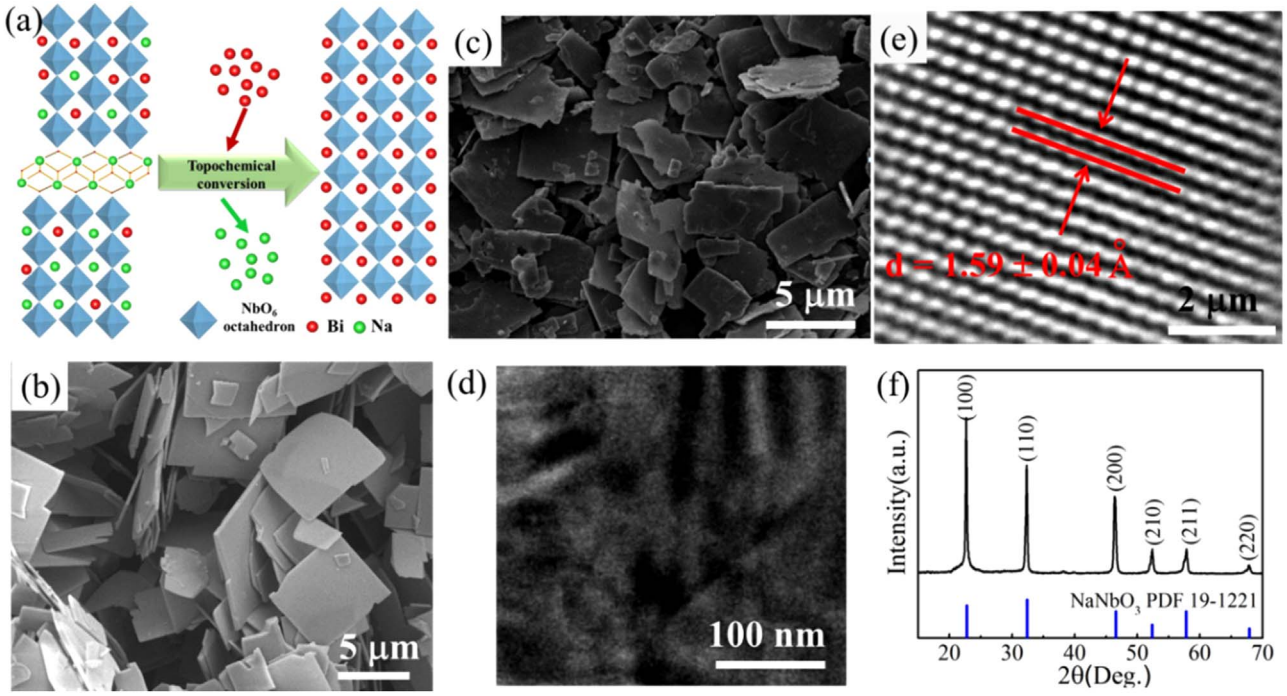

Fig. 2. Schematic illustration of topochemical conversion from BiNN5 precursors to 2D NN platelets (a); SEM images of BiNN5 (b) and 2D NN platelets (c); TEM bright field image of domain structure (d), HRTEM image (e), and XRD patterns of 2D NN platelets (f).

2.5. Finite element simulation

To further understand the newly structure design with the composites films effects on the electric field strength and leakage current density. The trilayered architecture and single layer composite films are further analyzed through finite element simulation (MATLAB and COMSOL Multiphysics). The NN two-dimensional platelets random distributions into the PVDF matrix have been generated via MATLAB. For the simulation system, the dielectric constant of NN two-dimensional platelets and PVDF is around 300 and 8.26. The conductivity of NN two-dimensional platelets and PVDF is around 10^{-8} S/m and 10^{-15} S/m.

3. Results and discussion

The 2D NN platelets were prepared by topochemical conversion of $Bi_{2.5}Na_{3.5}Nb_5O_{18}$ (BiNN5) platelets as precursors (Fig. 2(a)). First, BiNN5 platelets (dimensions 5–10 μm and thicknesses 0.3–0.7 μm) with a layered perovskite structure were synthesized via the molten-salt route. Then the BiNN5 precursors were transformed to 2D NN platelets through a topochemical reaction [46]. The 2D NN platelets have large aspect ratios, dimensions of 2–5 μm and thicknesses of 0.1–0.5 μm (Fig. 2(c)). The morphology and distribution of ferroelectric domains could be observed from the transmission electron microscopy (TEM) bright field image (Fig. 2(d)), where the dark and bright fringes represent the domains, with the domains and boundaries [49,50]. It is indicated the 2D NN platelets are typical ferroelectric materials. The d spacing estimated from the lattice fringe is 1.59 ± 0.04 Å (Fig. 2(e)), which corresponds well to the [210] crystal direction of the 2D NN platelets [46]. The 2D NN platelets possess a single-phase perovskite structure (Fig. 2(f)), indicating the layer-structured BiNN5 precursors have been completely converted into perovskite-structured 2D NN platelets.

A series of trilayered architecture NN/PVDF composite films were prepared by a solution casting layer-by-layer process, where the volume fraction of NN in the outer layer was 1, 3, 5, 9 and 13 vol%. The films were named as “x-0-x”, where x is the volume fraction of 2D NN platelets in the outer layers and 0 is the pristine PVDF in the middle layer. For example, the 1-0-1 refers to the trilayered architecture samples with 1 vol% 2D NN platelets in the outer layer and the middle layer is pristine PVDF. The top-view images of the outer layer and middle layer in the 3-0-3 film are shown in Fig. 3(c) and (d). Clearly, the 2D NN platelets are well dispersed into the polymer matrix with the help of the dense polymer surface layer of dopamine, which is about 8 nm thick (Fig. 3(a)). X-ray photoelectron spectroscopy (XPS) further confirms the successful coating of dopamine onto the NN surface (Fig. 3(b)). The thickness of the trilayered architecture films is about 15 μm, and each layer accounts for one third of the whole film (Fig. 3(e)). The trilayered films are welded very well at the interface, without any structure defects (e.g., voids or pores). The high preferred orientation indicates the majority of 2D NN platelets in the composite films were parallel to each other, due to the shearing force effect during the solution casting layer-by-layer process. This result means 2D NN platelets are effective at improving orientation quality through the process condition optimization, which is beneficial for improvement of dielectric performances and breakdown strength. The X-ray diffractometry (XRD) patterns of pristine PVDF, 2D NN platelets, and 3-0-3 composite film are illustrated in Fig. 3(f). The 3-0-3 composite film exhibits higher preferred orientation than the 2D NN platelets, and contains the α and γ phases of PVDF. The single-layer and trilayered architecture composite films both have phase structures consistent with pristine PVDF (Fig. S1), and have crystallinity degrees higher than pristine PVDF, which is because the 2D NN platelets act as heterogeneous nuclei in the crystalline nucleation (Fig. S2 and Table S1).

The frequency dependence of dielectric constant and dielectric loss for the pristine PVDF and trilayered architecture composite films is shown in Fig. 4(a) and (b). The trilayered architecture and single-layer composite films both show similar frequency-dependent dielectric behaviors as pristine PVDF (Fig. 4(a) and S3). The dielectric constant and dielectric loss significantly decrease at 10^6 Hz, which is ascribed to the dielectric relaxation in the PVDF matrix. The dielectric constant and dielectric loss gradually decrease with the increase of NN contents, because the crystallinity of composite films increases by incorporation of the 2D NN platelets as crystallization nuclei. In addition, the

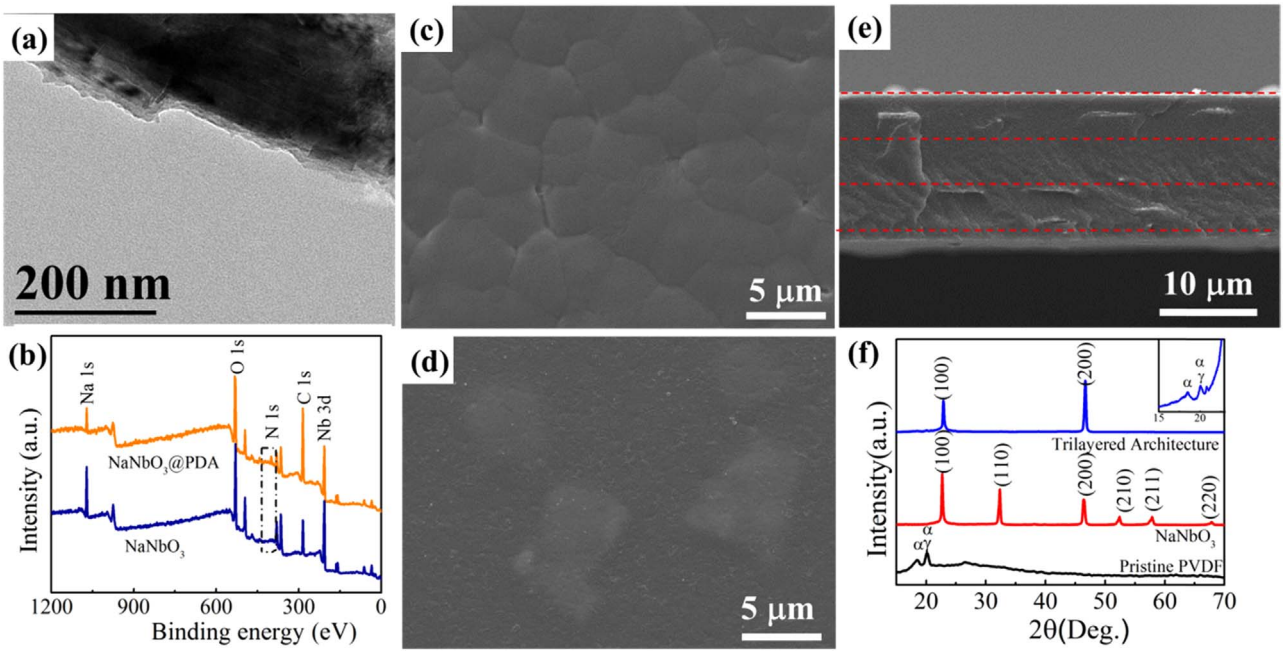

Fig. 3. (a) TEM images of 2D NN@PDA platelets; (b) XPS patterns of 2D NN and 2D NN@PDA platelets; top-view of (c) middle layer and (d) outer layer; (e) cross-section of 3-0-3 trilayered architecture composite film; (f) XRD patterns of pristine PVDF, 2D NN platelets, and 3-0-3 trilayered architecture composite film.

dielectric constant generally increases with the intensification of NN loading (Fig. 4(a)), because the 2D NN platelets have larger dielectric constant and aspect-ratio than the pristine PVDF. For example, with the loading of 13 vol% 2D NN platelets in the outer layers, the dielectric constant of the trilayered architecture composite films is up to 17.34 at 10^3 Hz. Compared with the single-layer composite films, the improvement of dielectric constant with trilayered architecture composite films is not as apparent at the similar condition since the relatively low dielectric constant of the middle layer. Meanwhile, the composite films with different NN volume fractions all maintain low dielectric loss (i.e., < 0.04 at 10^3 Hz), which is advantageous to low energy loss and small leakage current. As shown in Fig. 4(c), the current density of the trilayered architecture composite films measured at the applied electric field of 100 MV m^{-1} gradually increases with the increasing volume fraction of 2D NN platelets, due to the formation of more free electrons. The current densities of all trilayered architecture composite films maintain relatively low at about 8×10^{-7} A cm^{-2}, which contributes to improving the breakdown strength and energy density.

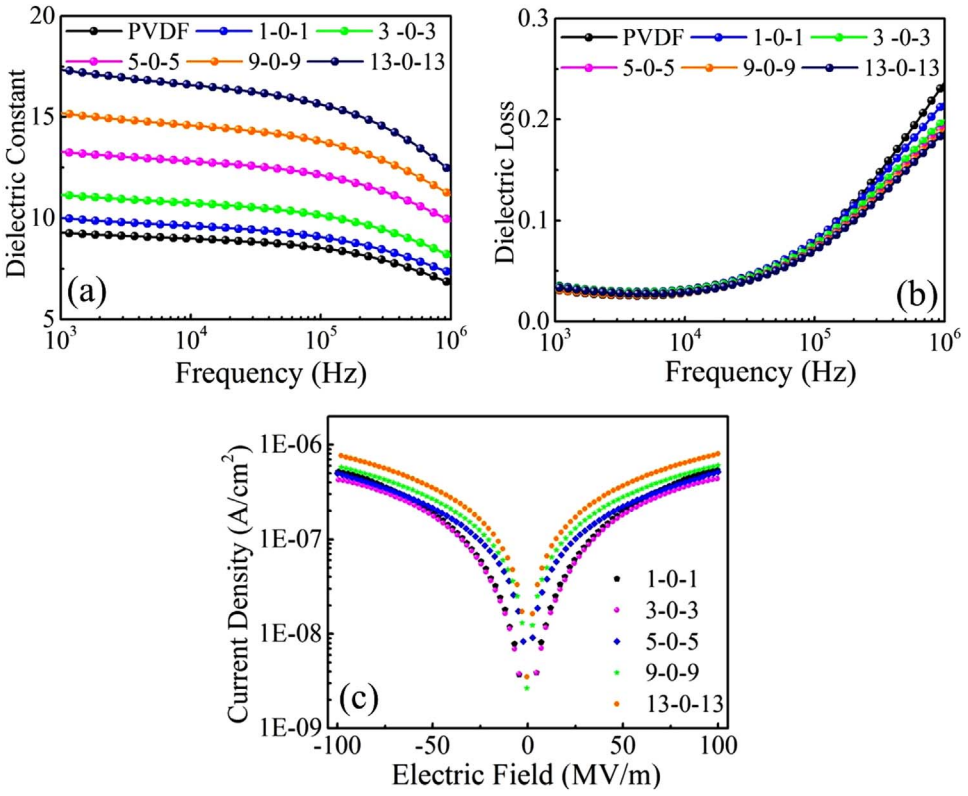

Fig. 4. Frequency-dependence of (a) dielectric constant, (b) dielectric loss and (c) current density of trilayered architecture composite films and pristine PVDF.

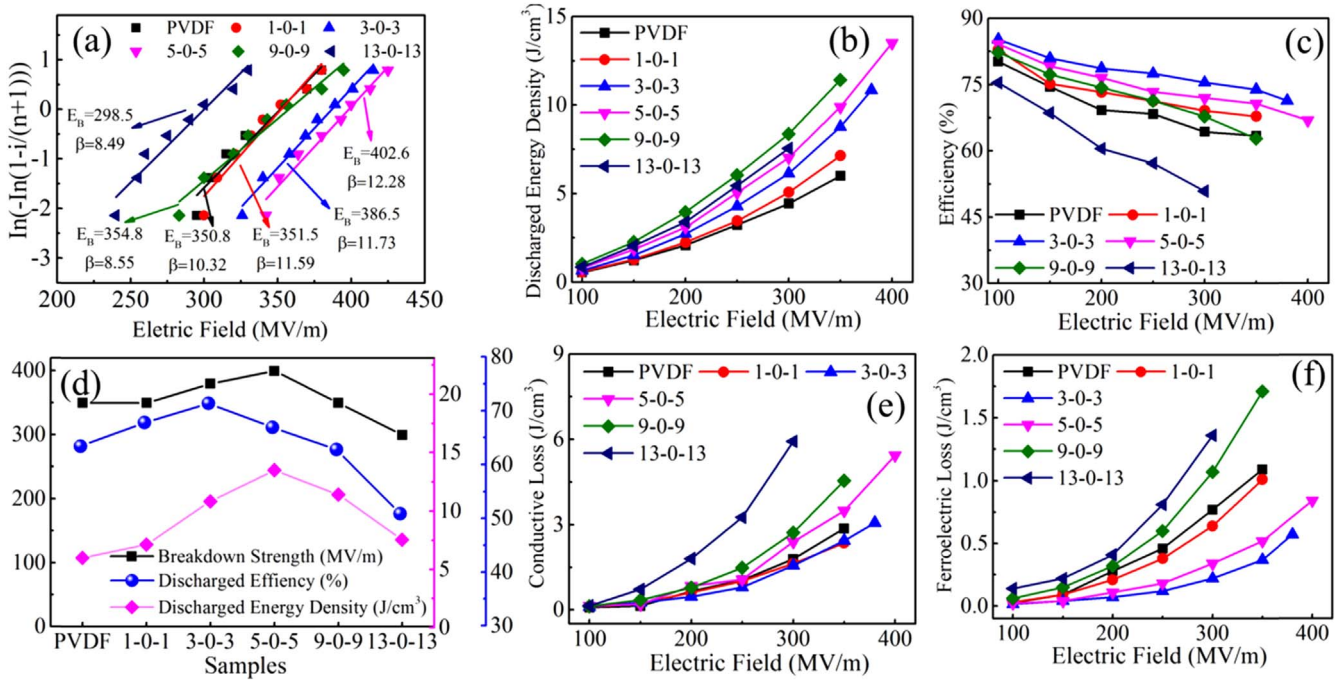

Fig. 5. (a) Weibull plots and deduced characteristic breakdown strength, (b) discharged energy density, (c) efficiency, (d) breakdown strength, discharged energy density, and discharged efficiency, (e) conductivity loss, and (f) ferroelectric loss of the trilayered architecture composite films and pristine PVDF.

The breakdown strength, which has an exponential influence on the charge storage capacity, is another critical metric of dielectric materials. Fig. 5(a) shows the Weibull plots of the breakdown strength of trilayered architecture composite films against the volume fraction of 2D NN platelets measured at room temperature. The Weibull statistic can be described as [51–54],

$$P(E) = 1 - \exp\left[-\left(\frac{E}{E_b}\right)^{\beta}\right]$$

where P(E) is the cumulative probability of electric failure, E is experimental breakdown strength, E_b is characteristic breakdown strength at the cumulative failure probability of 63.2%, and β is the shape parameter associated with the linear regressive fitting of data distribution. Clearly, the breakdown strength of the trilayered architecture composite films first increases obviously and then decreases with the increasing volume fraction of 2D NN platelets in the outer layers. The 5-0-5 trilayered architecture composite films has the highest breakdown strength of 400 MV m^{-1}, which is 14.3% higher than pristine PVDF (350 MV m^{-1}) and 25% higher than the corresponding single-layer composite film (300 MV m^{-1}). This result indicates the breakdown strength of trilayered architecture composite films could be improved significantly compared with the single-layer composite films.

To further elucidate the dependence of breakdown strength on the structure of nanocomposite films, we simulated the electric field strength of the 3-0-3 composite film and 3 vol% NN/PVDF (Fig. 6(a) and (b)). In the simulation systems (Fig. S4), the applied electric field from top to bottom gradually decreases from 9600 to 0 V (Fig. S5). Based on the electric potential distribution illustrated in Fig. S5, it is apparent that the redistribution of electric field is first deduced, and the distorted region was observed clearly. In addition, more equipotential line accumulates in the outer layer of the 3-0-3 composite films. The simulation results show the 3-0-3 composite film has a lower maximum electric field strength than the 3 vol% NN/PVDF composite film under the same applied electric field. This result indicates the 3 vol% NN/PVDF composite film breakdown more easily, which can be explained below. Incorporation of high-dielectric-constant 2D NN platelets into the outer layers could lead to the electric field redistribution, where the applied electric field is mostly distributed to the middle layer and a weak electric field region is formed in the outer layers. In other words, the middle layer undertakes higher electric field, which relieves the electric field strength in the outer layers. Therefore, the trilayered architecture composite films could tolerate a higher electric field than single-layer composite films at the same applied electric field. In addition, the strong interfacial barrier effect of between the outer layer and middle layer leads to much enhanced breakdown strength in trilayered architecture composites films. As shown in Fig. 6(a), a gap of electric field strength exists at the interfaces between the middle layer and outer layers of the 3-0-3 composite films, as indicated by the electric field distribution. Consequently, the developed breakdown channel in the outer layer, when passing through the middle layer, has to suffer from the weak electric field, and the sharp decrease of electric field strength is beneficial for blocking the breakdown channel around the interface. That is to say, the breakdown process could be easily promoted in the region with high electric field, while it develops difficultly in the region with low electric field. Detailed electric field strength of the internal composites is characterized, and the cross-section images of the composite film are illustrated in Fig. 6(c)-(f), with the model displayed in Fig. S6. Clearly, the local field near the two poles of an isolate particle along the field direction is the most enhanced, compared to the polymer matrix far away. The local field inside the 2D NN platelets is close to zero, which is attributed to the interfacial polarization due to the large dielectric constant contrast between the fillers and the polymer matrix. The adjacent fillers of the electric field form a channel or cluster together along the electric field, further enhancing the local field strength between these chained or clustered fillers. The formed electric field channel or cluster may be potentially the region of breakdown. In addition, the developed electric field channel is effectively prevented in the middle layer of the trilayered architecture composite films. We conclude from the simulation that the local field enhancement due to interfacial polarization, especially between chained or clustered fillers, accounts for decreased breakdown strength of single-layer polymer nanocomposites.

The typical electrical displacement dependence of electric field (D-E) curves of the trilayered architecture and single-layer composite films is illustrated in Fig. S7. The electrical displacement of the trilayered

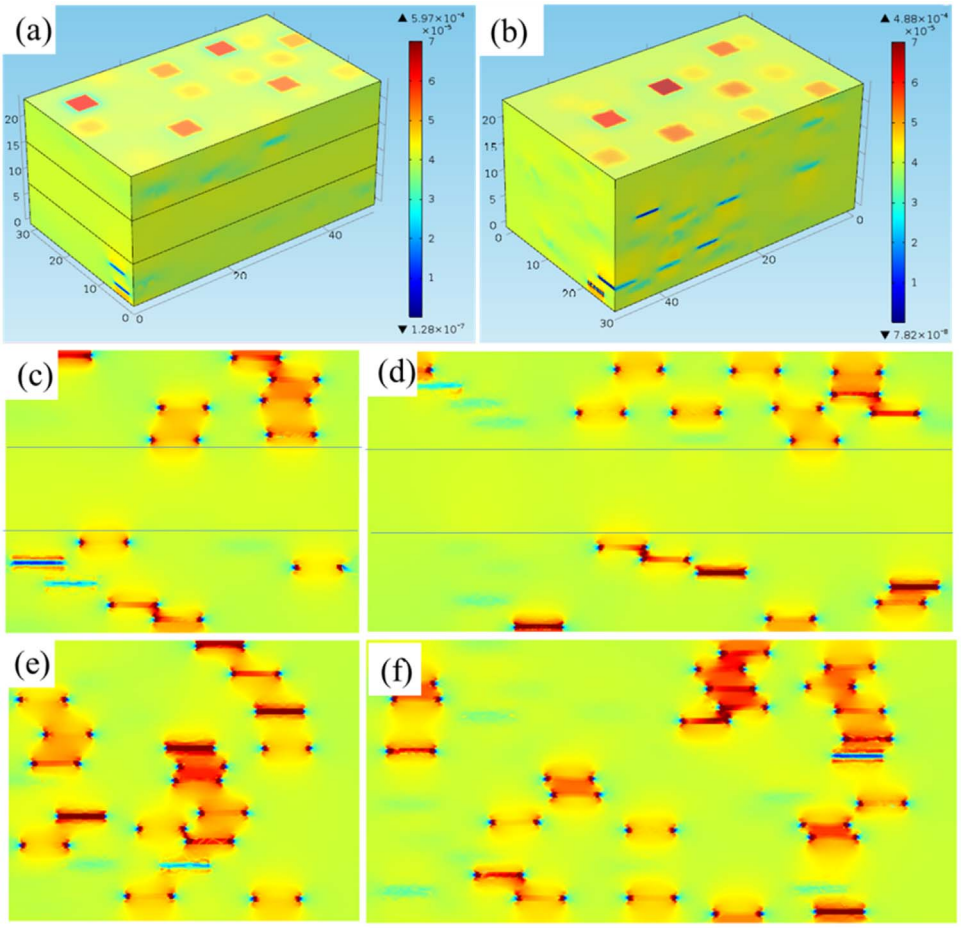

Fig. 6. Three-dimensional images of electric field strength of (a) 3-0-3 composite films and (b) 3 vol% NN/PVDF at the applied electric field of 6000 V; cross-section images of (c), (d) 3-0-3 composite films and (e), (f) 3 vol% NN/PVDF.

architecture composite films is enhanced sharply with the increase of volume fraction of 2D NN platelets under the same condition (Fig. S8). The discharge energy density and efficiency calculated by D-E curves are shown in Fig. 5(b) and (c). The discharge energy density and breakdown strength of trilayered architecture composite film have the same vary trend (Fig. 5(d)). The discharge energy density and breakdown strength of trilayered architecture composite films change in the same trend (Fig. 5(d)). With the highest breakdown strength and large polarization, the 5-0-5 composite film exhibits the largest discharge energy density of 13.5 J cm^{-3} at 400 MV m^{-1}, which is 125% higher than pristine PVDF (6 J cm^{-3}), and has discharge energy efficiency of 66.9%. Interestingly, the trilayered architecture composite film exhibits higher discharge energy density and discharge efficiency than the corresponding single-layer composite film (Figs. S9 and S10). The former could be ascribed to the larger breakdown strength and electric displacement, while the latter is mainly derived from the reduction of energy loss, which comprises of conductive loss (coming from conductivity and leakage current) and ferroelectric loss (from polarization hysteresis) [40,55].

To investigate the dielectric loss mechanism of the composite films, we derived conductive loss from the D–E curves, assuming that the polarization at zero field ($P_{E=0}$) comes mainly from the leakage current, given that the contents of polar phase in the investigated ferroelectric films are insignificant [3,40,56]. The effective conductivity (σ_{eff}) could be determined as follows [3,40,56]:

$$P_{E=0} = \frac{1}{2}\sigma_{eff} E_{max} T$$

where T is the period of the applied field. After σ_{eff} is determined, the conductive loss can be subtracted from the total dielectric loss to form the ferroelectric loss (Fig. 5(e) and (f)). For both pristine PVDF and trilayered architecture composite films, ferroelectric and conductive losses both are sharply intensified with the increase of the electric field. Additionally, conductive loss far surpasses ferroelectric loss in the trilayered films, indicating conductive loss plays a major role in the trilayered films. It is noted that the 3-0-3 composite film has the lowest ferroelectric loss and conductive loss, so it has the largest discharge efficiency of 71% (Fig. 7(b)). The ferroelectric loss and conductive loss of the pristine PVDF, single-layer, and trilayered architecture composite films also are shown in Fig. 7(c) and (d). Clearly, the conductive loss of the single-layer composite film significantly surpasses that of the pristine PVDF and the 3-0-3 composite film at the same electric field (Fig. 7(c)), due to the high conductivity of 2D NN platelets. In addition, the ferroelectric losses of single-layer and trilayered films are both lower than pristine PVDF at the same field (Fig. 7(d)), because the 2D NN platelets act as a nucleating agent in the composite films, resulting in the decrease of crystal size.

Finite element simulation was adopted to further evaluate how the structures of nanocomposite films affected the conductivity of composite films. The 3D images of leakage current density with 3-0-3 composite films and 3 vol% NN/PVDF are shown in Fig. 8(a) and (b). The contrast of leakage current density is mainly due to the difference of conductivity between the filler and the polymer matrix [57–59]. Moreover, the leakage current density of trilayered films is significantly lower than the single-layer composite films, which can be explained below. The 2D NN platelets with high conductivity lead to conduction redistribution, where the applied electric field is mostly added to the middle layer, and a weak conduction region appears in the outer layers. The cross-section leakage current densities of the 3-0-3 composite film and 3 vol% NN/PVDF are illustrated in Fig. 8(c)-(f), with the model displayed in Fig. S6. The 2D NN platelets possess higher conductivity

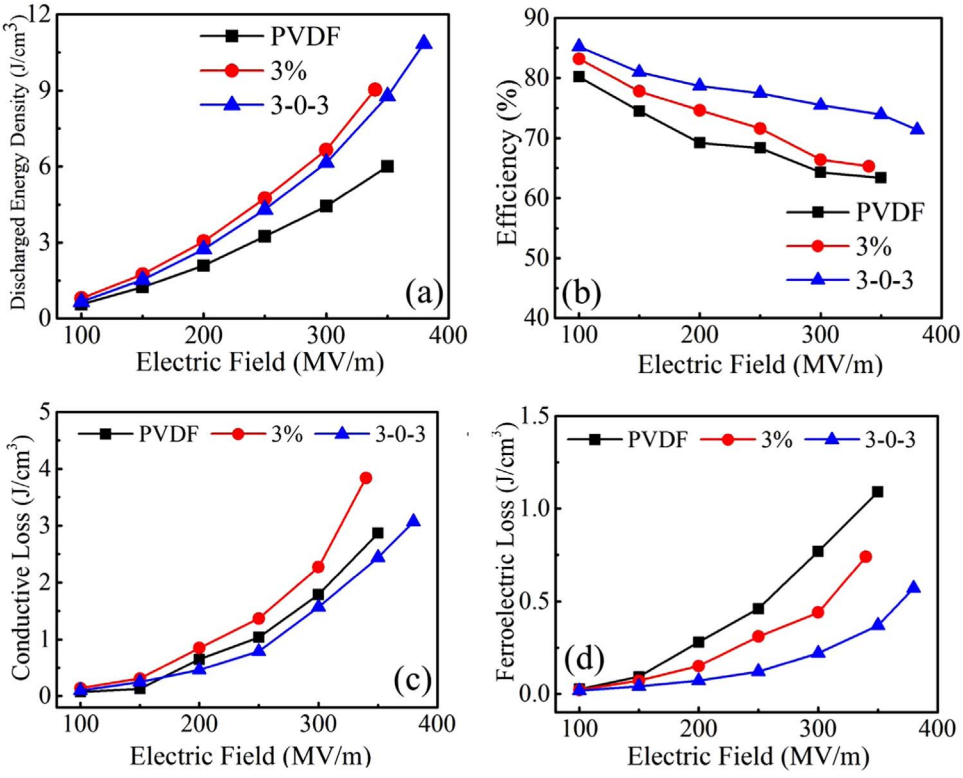

Fig. 7. (a) Discharged energy density, (b) efficiency, (c) conductive loss, and (d) ferroelectric loss of pristine PVDF, 3 vol% NN/PVDF, and 3-0-3 composite film.

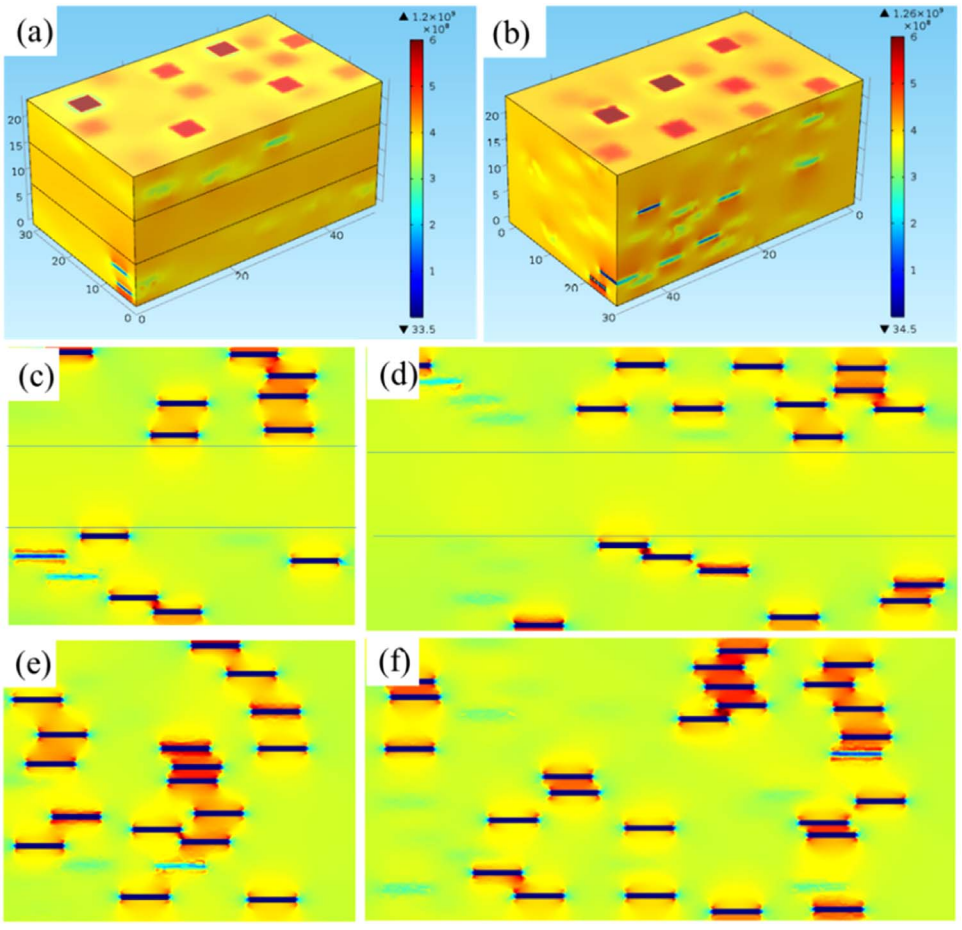

Fig. 8. Three-dimensional images of leakage current density of (a) 3-0-3 composite film and (b) 3 vol% NN/PVDF at the applied electric field of 6000 V; cross-section images of (c), (d) 3-0-3 composite film and (e), (f) 3 vol% NN/PVDF.

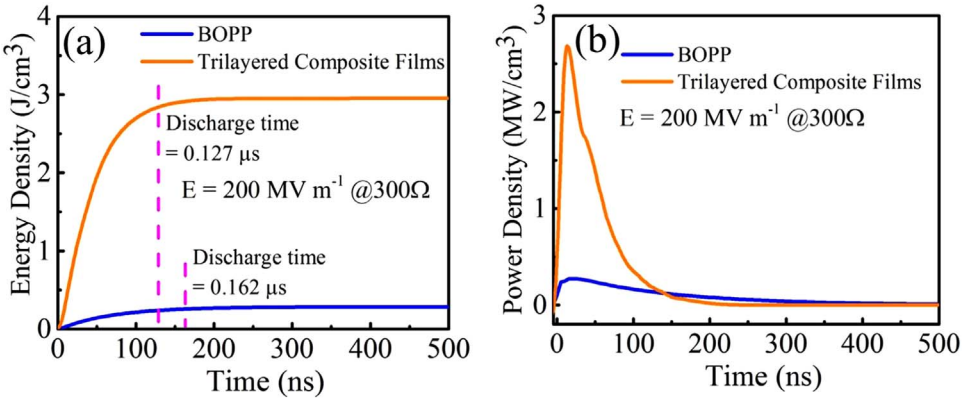

Fig. 9. Discharged energy density (a) and power density (b) of BOPP and the 5-0-5 composite film at the applied electric field of 200 MV m^{-1}.

than pristine PVDF. A larger amount of positive and negative charges accumulated at the upper and below region around the 2D NN platelets, forming a local high conduction region. The adjacent fillers form along the applied electric field a conduction channel region, which has higher leakage current density and may be a potential region of breakdown. These results further suggest the trilayered architecture composite films have larger breakdown strength than the single-layer composite films, which is consistent with the simulation of electric field strength.

The crucial parameters of capacitor devices in practical application include the energy density, power density, and charge-discharge speed. The charge-discharge speeds of BOPP and 5-0-5 composite film measured by resistor inductance capacitor (RLC) circuit are shown in Fig. S11 [1,60–63], charged at 200 MV m^{-1} and discharged across 300 Ω. As expected, the discharge rate of the 5-0-5 composite film is faster than commercial BOPP (about 0.127 vs. 0.162 μs) (Fig. 9(a)). The 5-0-5 composite film could discharge more density than BOPP (Fig. 9(a)) and exhibits a superior power density about ten times that of BOPP (2.68 vs. 0.27 MW cm^{-3}) (Fig. 9(b)). The excellent properties make the trilayered architecture composite films promising candidates for application into high-performance capacitor energy storage devices.

4. Conclusions

Trilayered architecture composite films comprised of two outer layers of 2D NN platelets dispersed in PVDF matrix to provide high dielectric constant and a middle layer of pristine PVDF to offer high breakdown strength. The breakdown strength, energy density, and discharge efficiency of the trilayered architecture composite films were improved significantly via tailoring the contents of 2D NN platelets. The trilayered film with 5 vol% NN has the highest discharge energy density of 13.5 J cm^{-3} at 400 MV m^{-1}, which is far higher than the pristine PVDF and commercial BOPP. Moreover, the composite films show a superior power density of 2.68 MW cm^{-3} and ultra-fast discharge speed of 0.127 μs. Finite element simulation further revealed the breakdown strength and energy density of the trilayered architecture composite films could be much enhanced compared to the corresponding single-layer composite films. The reasons of performance enhancement are that the middle layer in the trilayered architecture composite films could effectively relieve the electric field strength and energy loss. Thus, the novel structure design provides a new strategy to prepare high-performance electrostatic capacitor materials for application into high-power electronic and energy devices.

Acknowledgements

This work was supported by the Ministry of Science and Technology of China through 973-project under Grant (2015CB654601).

Appendix A. Supporting information

Supplementary data associated with this article can be found in the online version at http://dx.doi.org/10.1016/j.nanoen.2017.09.004.

References

[1] B. Chu, X. Zhou, K. Ren, B. Neese, M. Lin, Q. Wang, F. Bauer, Q.M. Zhang, Science 313 (2006) 334–336.
[2] Q. Li, L. Chen, M.R. Gadinski, S. Zhang, G. Zhang, H. Li, A. Haque, L.Q. Chen, T. Jackson, Q. Wang, Nature 523 (2015) 576–579.
[3] P. Khanchaitit, K. Han, M.R. Gadinski, Q. Li, Q. Wang, Nat. Commun. 4 (2013) 2845.
[4] Y. Shen, Y. Lin, Q.M. Zhang, MRS Bull. 40 (2015) 753–759.
[5] Q. Chen, Y. Shen, S. Zhang, Q.M. Zhang, Annu. Rev. Mater. Res. 45 (2015) 433–458.
[6] X. Chen, X. Han, Q.D. Shen, Adv. Electron. Mater. (2017) 1600460.
[7] Z.M. Dang, J.K. Yuan, S.H. Yao, R.J. Liao, Adv. Mater. 25 (2013) 6334–6365.
[8] L. Zhang, Z. Liu, X. Lu, G. Yang, X. Zhang, Z.Y. Cheng, Nano Energy 26 (2016) 550–557.
[9] Prateek, V.K. Thakur, R.K. Gupta, Chem. Rev. 116 (2016) 4260–4317.
[10] T.D. Huan, S. Boggs, G. Teyssedre, C. Laurent, M. Cakmak, S. Kumar, R. Ramprasad, Prog. Mater. Sci. 83 (2016) 236–269.
[11] X. Hao, J. Zhai, L.B. Kong, Z. Xu, Prog. Mater. Sci. 63 (2014) 1–57.
[12] Z.M. Dang, J.K. Yuan, J.W. Zha, T. Zhou, S.T. Li, G.H. Hu, Prog. Mater. Sci. 57 (2012) 660–723.
[13] W. Li, L. Jiang, X. Zhang, Y. Shen, C.W. Nan, J. Mater. Chem. A 2 (2014) 15803–15807.
[14] X. Huang, P. Jiang, Adv. Mater. 27 (2015) 546–554.
[15] E. Barshaw, J. White, M. Chait, J. Cornette, J. Bustamante, F. Folli, D. Biltchick, G. Borelli, G. Picci, M. Rabuffi, IEEE Trans. Magn. 43 (2007) 223–225.
[16] L. Xie, X. Huang, C. Wu, P. Jiang, J. Mater. Chem. 21 (2011) 5897.
[17] D. Yu, N. Xu, L. Hu, Q. Zhang, H. Yang, J. Mater. Chem. C 3 (2015) 4016–4022.
[18] Y. Xie, Y. Yu, Y. Feng, W. Jiang, Z. Zhang, ACS Appl. Mater. Interfaces 9 (2017) 2995–3005.
[19] X. Zhang, Y. Shen, B. Xu, Q. Zhang, L. Gu, J. Jiang, J. Ma, Y. Lin, C.W. Nan, Adv. Mater. 28 (2016) 2055–2061.
[20] D. Zhang, X. Zhou, J. Roscow, K. Zhou, L. Wang, H. Luo, C.R. Bowen, Sci. Rep. 7 (2017) 45179.
[21] L. Yao, Z. Pan, S.H. Liu, J. Zhai, H.H. Chen, ACS Appl. Mater. Interfaces 8 (2016) 26343–26351.
[22] Z.B. Pan, J.W. Zhai, B. Shen, J. Mater. Chem. A 5 (2017) 15217–15226.
[23] L. Yao, Z. Pan, J. Zhai, H.H. Chen, Nanoscale 9 (2017) 4255–4264.
[24] Y. Yang, B. Zhu, D. Yin, J. Wei, Z. Wang, R. Xiong, J. Shi, Z. Liu, Q. Lei, Nano Energy 17 (2015) 1–9.
[25] Z. Pan, L. Yao, J. Zhai, B. Shen, H. Wang, Compos. Sci. Technol. 147 (2017) 30–38.
[26] G. Wang, X. Huang, P. Jiang, J. Mater. Chem. C 5 (2017) 3112–3120.
[27] Y. Hao, X. Wang, K. Bi, J. Zhang, Y. Huang, L. Wu, P. Zhao, K. Xu, M. Lei, L. Li, Nano Energy 31 (2017) 49–56.
[28] Z.M. Dang, M.S. Zheng, J.W. Zha, Small 12 (2016) 1688–1701.
[29] Z. Pan, L. Yao, J. Zhai, K. Yang, B. Shen, H. Wang, A.C.S. Sustain, Chem. Eng. 5 (2017) 4707–4717.
[30] Q. Li, G. Zhang, F. Liu, K. Han, M.R. Gadinski, C. Xiong, Q. Wang, Energy Environ. Sci. 8 (2015) 922–931.
[31] Q. Li, K. Han, M.R. Gadinski, G. Zhang, Q. Wang, Adv. Mater. 26 (2014) 6244–6249.
[32] L. Zhang, Z.Y. Cheng, J. Adv. Dielectr. 1 (2011) 389–406.
[33] X. Zhang, Y. Shen, Q. Zhang, L. Gu, Y. Hu, J. Du, Y. Lin, C.W. Nan, Adv. Mater. 27 (2015) 819–824.
[34] B. Xie, H. Zhang, Q. Zhang, J. Zang, C. Yang, Q. Wang, M.Y. Li, S. Jiang, J. Mater. Chem. A 5 (2017) 6070–6078.
[35] H. Tang, Z. Zhou, H.A. Sodano, ACS Appl. Mater. Interfaces 6 (2014) 5450–5455.
[36] S.P. Fillery, H. Koerner, L. Drummy, E. Dunkerley, M.F. Durstock, D.F. Schmidt,

R.A. Vaia, ACS Appl. Mater. Interfaces 4 (2012) 1388–1396.
[37] P. Hu, J. Wang, Y. Shen, Y. Guan, Y. Lin, C.-W. Nan, J. Mater. Chem. A 1 (2013) 12321.
[38] P. Hu, Y. Shen, Y. Guan, X. Zhang, Y. Lin, Q. Zhang, C.W. Nan, Adv. Funct. Mater. 24 (2014) 3172–3178.
[39] Y. Wang, J. Cui, Q. Yuan, Y. Niu, Y. Bai, H. Wang, Adv. Mater. 27 (2015) 6658–6663.
[40] Y. Wang, J. Cui, L. Wang, Q. Yuan, Y. Niu, J. Chen, Q. Wang, H. Wang, J. Mater. Chem. A 5 (2017) 4710–4718.
[41] Y. Shen, D. Shen, X. Zhang, J. Jiang, Z. Dan, Y. Song, Y. Lin, M. Li, C.W. Nan, J. Mater. Chem. A 4 (2016) 8359–8365.
[42] Y. Wang, Y. Hou, Y. Deng, Compos. Sci. Technol. 145 (2017) 71–77.
[43] F. Liu, Q. Li, J. Cui, Z. Li, G. Yang, Y. Liu, L. Dong, C. Xiong, H. Wang, Q. Wang, Adv. Funct. Mater. 27 (2017) 1606292.
[44] Y. Shen, Y. Hu, W. Chen, J. Wang, Y. Guan, J. Du, X. Zhang, J. Ma, M. Li, Y. Lin, L. Chen, C.W. Nan, Nano Energy 18 (2015) 176–186.
[45] C.R. Dean, A.F. Young, I. Meric, C. Lee, L. Wang, S. Sorgenfrei, K. Watanabe, T. Taniguchi, P. Kim, K.L. Shepard, J. Hone, Nat. Nanotechnol. 5 (2010) 722–726.
[46] M. Kroutvar, Y. Ducommun, D. Heiss, M. Bichler, D. Schuh, G. Abstreiter, J.J. Finley, Nature 432 (2004) 81–84.
[47] L. Chao, Y. Hou, M. Zheng, Y. Yue, M. Zhu, Appl. Phys. Lett. 110 (2017) 122901.
[48] W. Bai, D. Chen, P. Zheng, J. Xi, Y. Zhou, B. Shen, J. Zhai, Z. Ji, J. Eur. Ceram. Soc. 37 (2017) 2591–2604.
[49] C. Jiang, D. Zhang, K. Zhou, X. Zhou, H. Luo, I. Abrahams, J. Mater. Chem. A 4 (2016) 18050–18059.
[50] R. Dittmer, W. Jo, J. Roedel, S. Kalinin, N. Balke, Adv. Funct. Mater. 22 (2012) 4208–4215.
[51] Z. Pan, L. Yao, J. Zhai, B. Shen, S. Liu, H. Wang, J. Liu, J. Mater. Chem. A 4 (2016) 13259–13264.
[52] H. Luo, J. Roscow, X. Zhou, S. Chen, X. Han, K. Zhou, D. Zhang, C.R. Bowen, J. Mater. Chem. A 5 (2017) 7091–7102.
[53] S. Luo, Y. Shen, S. Yu, Y. Wan, W.-H. Liao, R. Sun, C.P. Wong, Energy Environ. Sci. 10 (2017) 137–144.
[54] A. Kishimoto, Kunihito Koumoto, Hiroaki Yanagida, J. Mater. Sci. 24 (1989) 698–702.
[55] Q. Li, Q. Wang, Macromol. Chem. Phys. 217 (2016) 1228–1244.
[56] Q. Chen, Y. Wang, X. Zhou, Q.M. Zhang, S. Zhang, Appl. Phys. Lett. 92 (2008) 142909.
[57] Z. Pan, L. Yao, J. Zhai, D. Fu, B. Shen, H. Wang, ACS Appl. Mater. Interfaces 9 (2017) 4024–4033.
[58] R.J. Fleming, IEEE Trans. Dielectr. Electr. Insul. 12 (2005) 967–978.
[59] S.T. Li, G.L. Yin, G. Chen, J.Y. Li, S. Bai, L.S. Zhong, Y.X. Zhang, Q.Q. Lei, IEEE Trans. Dielectr. Electr. Insul. 17 (2010) 1523–1636.
[60] H. Tang, H.A. Sodano, Nano Lett. 13 (2013) 1373–1379.
[61] Z. Pan, L. Yao, J. Zhai, H. Wang, B. Shen, ACS Appl. Mater. Interfaces 9 (2017) 14337–14346.
[62] Z.B. Pan, L.M. Yao, J.W. Zhai, S.H. Liu, K. Yang, H.T. Wang, J.H. Liu, Ceram. Int. 42 (2016) 14667–14674.
[63] F. Li, K. Yang, X. Liu, J. Zou, J.W. Zhai, B. Shen, P. Li, J. Shen, B.H. Liu, P. Chen, K.Y. Zhao, H.R. Zeng, Scr. Mater. 141 (2017) 15–19.

Zhongbin Pan is a Ph.D. candidate of materials science and engineering at Tongji University. His research interests focus on the nanomaterials synthesis, advance structural materials, multifunctional materials, ferroelectric and dielectric materials, especially polymer nanocomposites for dielectric energy storage applications.

Baihui Liu is currently a Master candidate in the School of Materials Science and Engineering at Tongji University. Her research interests focus on dielectric, ferroelectric, piezoelectric ceramic materials and their applications.

Jiwei Zhai is a Professor in School of Materials Science and Engineering at Tongji University. He received his Ph.D degree from School of Electronic & Information Engineering, Xi'an Jiaotong University in 1997. His research interests focus on the electronic materials and devices, including the research of information functional materials and devices, temperature sensor, nano materials and devices, ferroelectric thin films, high-energy-density dielectric capacitors.

Lingmin Yao is an Associate Professor in School of Physics and Electronic Engineering at Guangzhou University. She received her Ph.D degree from Institute of Applied Physics and Materials Engineering, University of Macau in 2017. Her scientific interests focus on nanomaterials synthesis, advance structural materials, multifunctional materials, ferroelectric and dielectric materials, especially nanorod array application of functional nanodevices.

Ke Yang is currently a Master candidate in the School of Materials Science and Engineering at Tongji University. His research interests focus on glass-ceramic for application in dielectric capacitors.

Bo Shen is an Associate Professor in School of Materials Science and Engineering at Tongji University. She received her B.S. and M.S. degree from School of Electronic & Information Engineering, Xi'an Jiaotong University. Her research interests focus on dielectric, ferroelectric, piezoelectric ceramic materials and their applications.